Electron paramagnetic resonance tagged High Resolution Excitation Spectroscopy of NV-Centers in 4H-SiC

S. Zargaleh, H. von Bardeleben, J. Cantin, U. Gerstmann, S. Hameau, B. Eble, Weibo Gao

EPR tagged High Resolution Excitation Spectroscopy of NV- Centers in 4H-SiC

S.A. Zargaleh,[1] H.J. von Bardeleben,[2,*] J.L. Cantin,[2] U. Gerstmann,[3,†] S. Hameau,[2] B. Eblé,[2] and Weibo Gao[1,4]

[1] *Division of Physics and Applied Physics, School of Physical and Mathematical Sciences, Nanyang Technological University, Singapore 637371, Singapore*[‡]

[2] *Sorbonne Université, Campus Pierre et Marie Curie, Institut des Nanosciences de Paris, 4, place Jussieu, 75005 Paris, France*

[3] *Lehrstuhl für Theoretische Physik, Universität Paderborn, Warburger Strasse 100, 33098 Paderborn, Germany*

[4] *The Photonics Institute and Centre for Disruptive Photonic Technologies, Nanyang Technological University, Singapore 637371, Singapore*

(Dated: October 17, 2018)

We show that Electron Paramagnetic Resonance (EPR) tagged high resolution photoexcitation spectroscopy is a powerful method for the correlation of zero phonon photoluminescence spectra with atomic point defects. Applied to the case of NV centers in 4*H*-SiC it allows to associate the photoluminescence zero phonon lines (ZPL) at 1243 nm, 1223 nm, 1180 nm, 1176 nm with the (hk, kk, hh, kh) configurations of the NV^-centers in this material. These results lead to a revision of a previous tentative assignment. Contrary to theoretical predictions, we find that the NV centers in 4*H*-SiC show a negligible Franck-Condon shift as their ZPL absorption lines are resonant with the ZPL emission lines. The high sub-nanometer energy resolution of this technique allows us further to resolve additional fine structure of the ZPL lines of the axial NV centers which show a doublet structure with a splitting of 0.8 nm. Our results confirm that NV centers in 4*H*-SiC provide strong competitors for sensing and qubit application due to the shift of their optical transitions into the technology compatible near infrared region and the superior material properties of SiC. Given that single center spin readout will be realized, they are suitable for scalable nanophotonic devices compatible with optical communication network.

I. INTRODUCTION

In diamond, negatively charged carbon vacancy-nitrogen close pairs $(N_CV_C)^-$, the so-called NV centers, have shown to be exceptional candidates for application as solid-state qubits and for localized nano-sensing of magnetic fields, electric fields and temperatures[1]. Due to the superior material properties of 4*H*-SiC, a mature microelectronic material routinely applied in high frequency and high power devices, NV centers in this material can be expected to be challenging competitors for standard diamond-based qubits[2–7] and offer in addition the possibility of large-scale integration in microelectronic devices. Recent results obtained for silicon vacancies and silicon-carbon divacancy defects in SiC have shown that indeed they have promising magneto-optical properties. Room temperature coherent control of single spins, resonant addressing and manipulation of silicon vacancy qubits, room temperature quantum entanglement, long lived quantum memories as well as nanoscale temperature sensing have all been demonstrated for these defects[8–15]. The more recently evidenced NV centers in SiC can be expected to hold similar promising properties and the results presented in our previous work confirm these expectations.

In this study we apply a refined approach for linking ZPL emission lines directly with atomic defects. This technique, combining electron paramagnetic resonance (EPR) spectroscopy and high resolution (0.1 nm) *wavelength-scanning* resonant optical excitation, should find wide application in the field of solid state qubits in semiconductors in general. Note that resonant excitation spectroscopy via EPR had also been reported for the Si vacancy centers in 6*H*-SiC[8,16,17] and 15*R*-SiC[18].

NV centers in 4*H*-SiC are close pair silicon vacancy-nitrogen defects $(N_CV_{Si})^-$,[19] which in their negative charge state have magneto-optical properties similar to those of NV centers in diamond with a spin $S = 1$ ground state (GS), a spin $S = 1$ excited state (ES) and an intermediate singlet state (IS). Whereas NV centers in diamond have been studied in great detail their counterparts in 4*H*-SiC have only been assessed recently[20–24].

As the band-gap and crystal symmetry of 4*H*-SiC are different from the case of diamond, the NV center proper-

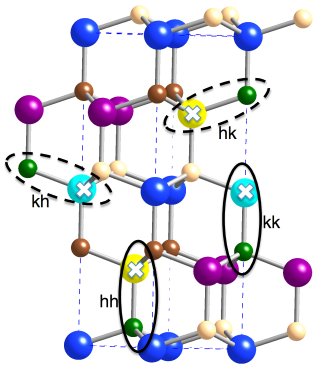

FIG. 1. Crystal structure and atomic model of the four different NV centers in 4*H*-SiC; Si atoms on k and h sites are shown blue and magenta and carbon atoms as small brown and beige balls; the Si vacancies on the k and h sites are shown in light blue and yellow and the Nitrogen atoms as small green balls.

TABLE I. Experimental and calculated NV center related ZPL emission energies/wavelength according to previous (tentative) assignment to the NV center configurations ('*old* model') taken from Ref. 21; theoretical values from the same reference and from Ref. 23. Besides the four NV related ZPL, two further lines (PLX5 and PLX6) have been assumed in Ref. 21 to belong to tungsten (W_{Si}) impurities.

label	PLX1	PLX2	PLX3	PLX4	PLX5/6
exp. ZPL (eV) (nm)	0.998 1242	0.999 1241	1.014 1223	1.051 1180	1.056 1176
old model	kk	hh	hk	kh	W_{Si}
DFT [18] (eV) (nm)	0.97 1278	0.99 1252	1.00 1240	1.02 1215	
DFT [20] (eV) (nm)	1.018 1218	0.966 1283	1.039 1193	1.056 1174	

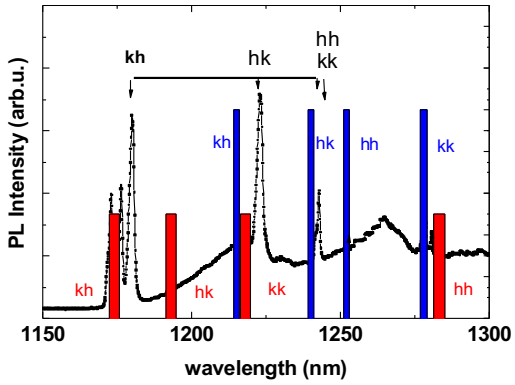

FIG. 2. Low temperature photoluminescence spectrum of 4*H*-SiC displaying the ZPL lines observed in the spectral region 1160 nm to 1260 nm and their assignment to the NV centers proposed in Ref. 21 (*black*); equally shown the theoretical prediction for the ZPL emisson energies from the same reference obtained within constrained DFT for a 432-atom supercell and a shifted $2 \times 2 \times 2$ *k*-point sampling[21] (*blue*) and for a 576-atom cell using the Γ-point approximation[23] (*red*). In both cases the HSE hybrid functional has been applied.

ties are of course modified. The lower crystal symmetry of 4*H*-SiC leads to different type of nonequivalent NV centers, which are distinguished by the lattice site of the silicon vacancy and the neigboring nitrogen atom. In 4*H*-SiC we have two non-equivalent lattice sites, which are called quasicubic (k) and hexagonal (h) and differ in their second neighbor configurations. Just as in the case of substitutional impurities, such as Nitrogen donors and Boron acceptors, this introduces distinct electronic properties which depend on their lattice site[16]. As NV centers are close pair defects, two non-equivalent sites (Fig. 1) give rise to a total of four distinct NV centers[22,23]. If the N neighboring atom is on-axis, i.e. the defect symmetry axis is parallel to the crystal *c*-axis, the center is called an *axial* NV center with C_{3v} symmetry (direct equivalent symmetry to NV in diamond). If the N atom is situated in the (0001) plane the defect symmetry is C_{1h} and the center is called *basal* NV center. Their physical properties are nevertheless quite similar[20–24]. One major difference from NV centers in diamond is the fact that their optical intra-center transitions between the ground state and the first excited state are no longer situated in the visible, but shifted in the NIR region[21], a wavelength range more suitable for transmission in optical fibers. A second important difference is the all-parallel orientation of the axial NV centers (Fig. 1), which allows to prevent a mixture of differently oriented qubits.[21]. This might be particularly advantageous for nano-sensing applications with large ensembles of NV centers. As we have four distinct NV centers in 4*H*-SiC, we should observe also four ZPL emission lines corresponding to the radiative recombination from the first excited state. The assignment of the zero-phonon photoluminescence lines with a particular NV center configuration is not straightforward. In previous publications[21,22], based on first principles calculations of their energies and also motivated by strong similarities to the divacancy which has a similar electronic structure[6,20], we have tentatively assigned the four ZPL lines to the respective NV centers (kk, hh, hk, kh within energy-increasing order; cf. Table I). However, given the precision with which such energies could be calculated and given the small differences of the ZPL energies[25,26] this assignment could not be considered as conclusive (cf. Fig. 2).

In order to further investigate this assignment, we have undertaken high resolution wavelength-scanning resonant photoexcitation EPR measurements, which have allowed us to refine these assignments. This method is complementary to optically detected magnetic resonance (ODMR) spectroscopy as it reveals due to the resonant excitation of the ZPL photoluminescence spectra the fine structure of the electronic states. It overcomes also the technical problems associated with an all-optical approach in which the overlap of excitation and emission spectra render such measurements difficult or impossible. Our approach is based on the selectivity of the NV center configurations in EPR spectroscopy. As the negatively charged NV centers have distinct Spin Hamiltonian parameters, they can be measured separately by EPR spectroscopy and their excitation spectrum is directly obtained by the photo EPR measurements.

II. EXPERIMENTAL

A. Photo-EPR Spectroscopy and PL Spectroscopy

For this study we used commercially purchased n-type conducting nitrogen doped 4H substrates. Contrary to the case of divacancy centers, NV centers are not present in these samples before any treatment. We have introduced NV centers with the process already described in Ref. 20 and 21. First, Si monovacancies are generated by high energy particle (proton) irradiation, followed by a thermal annealing at 800°C. At this temperature the Si monovacancies become mobile, diffuse and form close pair complexes with the stable nitrogen N centers. The same samples of typical dimensions of 3×4 mm^2 were used for both the photoluminescence and the EPR measurements in order to correlate the PL spectra with the different centers. The photoluminescence spectra were measured at T=10 K with non resonant excitation of 1000 nm. The excitation was focussed on to the sample with a 0.5 NA microscope objective. The photoluminescence was dispersed by a 0.5 m focal length monochromator with a spectral resolution of 0.04 meV and detected with an InGaAs diode. The EPR spectra were measured with a Bruker X-band spectrometer at 9.3 GHz and magnetic field modulation at 100 kHz. Due to the small linewidth (300 mG) of NV centers in SiC, the modulation amplitude was set to 0.125 G. All EPR measurements were performed at T=4 K. At this temperature the EPR spectra are observed as absorption spectra due to the passage conditions. For the high resolution EPR excitation measurements the samples were photoexcited in situ. The excitation source was a single mode tunable diode laser (Sacher Laser Technik), which could be tuned between 1170 nm and 1260 nm in steps of 0.01 nm and had a linewidth of 100 kHz. The output power was 30 mW. Due to the long spin lattice relaxation times of the order of min, each photoexcitation measurement was followed by a reset period of some minutes.

III. RESULTS

In this section we will present first (*i*) our experimental results of the photoluminescence spectra obtained with low and high spectral resolution under non resonant excitation, (*ii*) typical EPR spectra of the four NV centers and their angular variations and finally (*iii*) the photo induced variation of the intensity of the EPR spectrum of each of the four NV center when scanning the excitation in the range 1170 nm to 1260 nm over the different zero phonon PL lines. We have shown previously in Ref. 20, that the photoexcitation of the first excited ^{3}E state will lead to a spin polarization of the ground state (GS) with a strongly increased population of the m_s=0 state as compared to its thermal equilibrium value. This effect will be used to monitor the optical absorption spectra of each NV center.

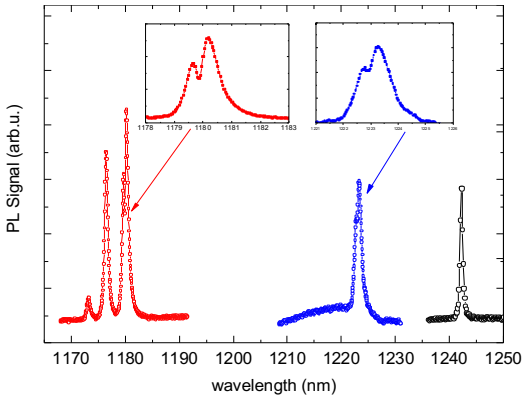

FIG. 3. Low temperature high resolution PL spectrum of the NV center related ZPL and (*insert*) zoom of the doublet structures observed for the ZPL at 1223 nm and 1180 nm.

A. High Resolution PL Spectroscopy

When excited with photons of energies in the range 800 nm to 1000 nm the samples display a weak four line ZPL spectrum in the 1080 nm to 1140 nm range, previously associated with the ZPL lines of the $^3\mathrm{E} \rightarrow {}^3\mathrm{A}_2$ transition of the neutral divacancies[27] and four high intensity ZPL lines between 1160 nm and 1250 nm as shown in Fig. 2. These ZPL at 1243 nm, 1223 nm, 1180 nm, 1176 nm have been previously associated with the NV centers[21] and a transition metal (W) contamination respectively. This tentative assignment was primarily based on a comparison with results obtained from first principal calculations[20–23], but also motivated by strong similarities to the divacancy which has a similar electronic structure[6,20] and the same order of ZPL lines (kk, hh, hk, kh within energy-increasing order). Hence, this assignment could not be considered as definitive. In the following we will restrict on experimental results, preventing the refined assignment from any uncertainties within calculated ZPL energies. Thereby, we will focus in particular on the ZPL lines at 1243 nm, 1223 nm, 1180 nm, 1176 nm, which, as we will show later, are indeed associated with the four NV centers. Due to a higher resolution of these PL measurements, we observe further, that two of the ZPL lines (1223 nm, 1180 nm) are split into doublets with a separation of 0.8 nm (Fig. 3).

B. High Resolution EPR Spectroscopy

In Fig. 4 we show a large scale EPR spectrum for the orientation of the magnetic field B//c-axis displaying simultaneously the respective spectra of the two axial and basal NV centers. As the negativly charged NV centers have a spin S=1 groundstate each NV center will give rise to a two line spectrum for this orientation. This spectrum was measured under photoexcitation and at low temperature (T=4 K); in this case all EPR lines have an absorp-

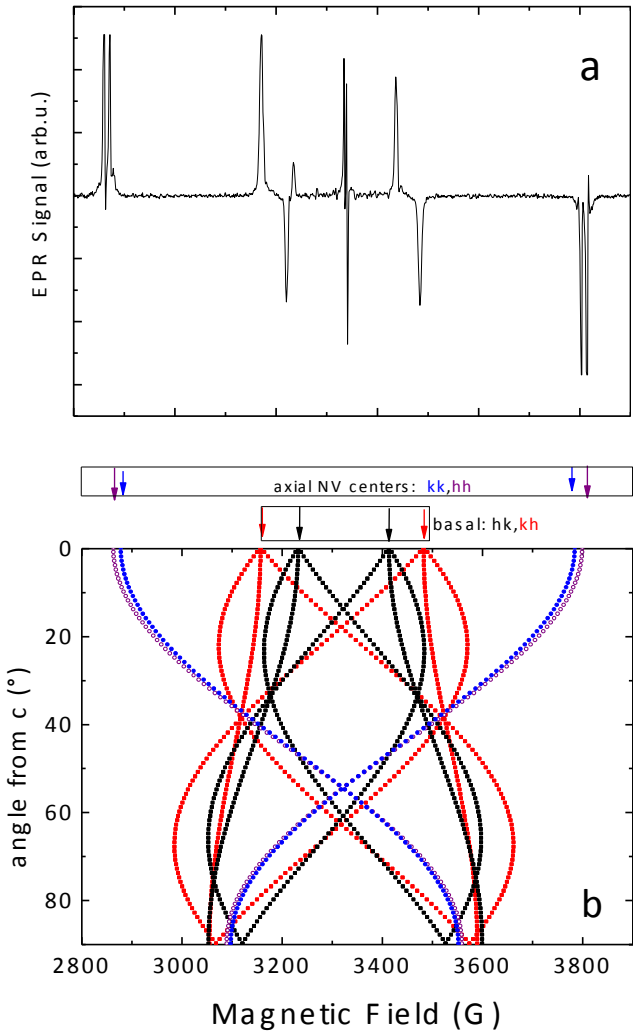

FIG. 4. *top (a)*: EPR spectrum in 4*H*-SiC for B//*c* at T=4 K showing the distinct spectra of the four (kk, hh, kh, hk) NV centers. *bottom (b)*: angular variation of the resonance fields of the axial (*large* ZFS) and basal (in this rotation plane *smaller* ZFS) NV centers for a rotation of the magnetic field in the $(11\bar{2}0)$ plane. For the orientation of the applied magnetic field parallel to the crystal *c*-axis the resonance fields of the four NV centers are sufficently separated to allow a selective study of their excitation properties. This orientation is employed in this study.

tion lineshape due to the passage conditions. Because of their different point symmetries (C_{3V} and C_{1h} respectively) and different Spin Hamiltonian parameters[20,22,23], the resonance fields of each of the four centers are well separated. In Fig. 4b we also show the angular variation of the resonance fields of the four NV centers for a rotation of the applied magnetic field in the $(11\bar{2}0)$ plane. For the photoexcitation measurements we will use in particular the orientation of the applied magnetic field parallel to the *c*-axis, for which the low field lines of the axial NV centers are at 2867 G and 2884 G and the basal ones at 3174 G and 3237 G.

As shown previously in Ref. 20 the photoexcitation into the first excited state allows for a high degree of groundstate spin polarization close to 100%. By this the EPR signal intensities are increased and the phases of the low and high field lines are changed into absorption and emission, respectively (see also Fig. 4a). In the following we have used the low field lines to monitor the EPR signal intensity as a function of the excitation wavelength. Thus, by measuring separately the EPR line intensity of each center as a function of excitation photon energy, we are able to identify the ZPL line associated with the EPR signature of each individual NV center (kk, hh, hk, kh).

1. *High Resolution On-Resonance Excitation*

Of the four NV centers the axial centers (hh and kk) with $E = 0$ show the largest D-values. Let us illustrate in more detail for the case of one of these centers, the NV(kk) center, the way we proceed with the photoexcitation measurements. The EPR measurements are done with the magnetic field aligned parallel to the crystal *c*-axis. For this orientation the resonance fields of the EPR transitions of the four NV centers are well separated and allow us the analysis of each NV center separately, cf. Fig. 4. We then select the field range corresponding to the resonance of the NV(kk) center (2875 G ±5 G). For each excitation wavelength we measure the intensity of the EPR spectrum and analyze the change induced by the excitation. Before changing the excitation wavelength to the next value we allow the defect to relax back to its thermal equilibrium value. In Fig. 5 we show the photoexcitation spectrum of the kk center measured in this way with low spectral resolution. Contrary to our expectation we do not observe any photoinduced variation while scanning the excitation around the zero phonon line at 1243 nm, previously associated with the kk center[21].

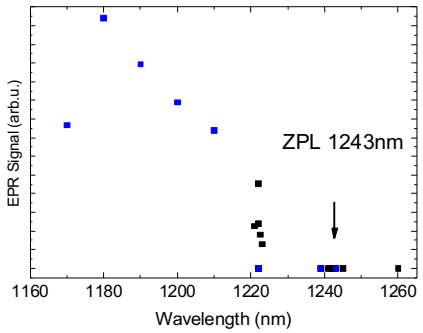

FIG. 5. Large scale, off-resonant photoexcitation EPR spectrum of the axial NV(kk) center. This center is not excited at 1243 nm (previous tentative assignment[21]), but shows a threshold close to 1223 nm. The apparently larger spin-polarization in the sideband than in ZPL excitation is due to the narrow linewidth of the ZPL, which is below the resolution in this lower-resolution measurements.

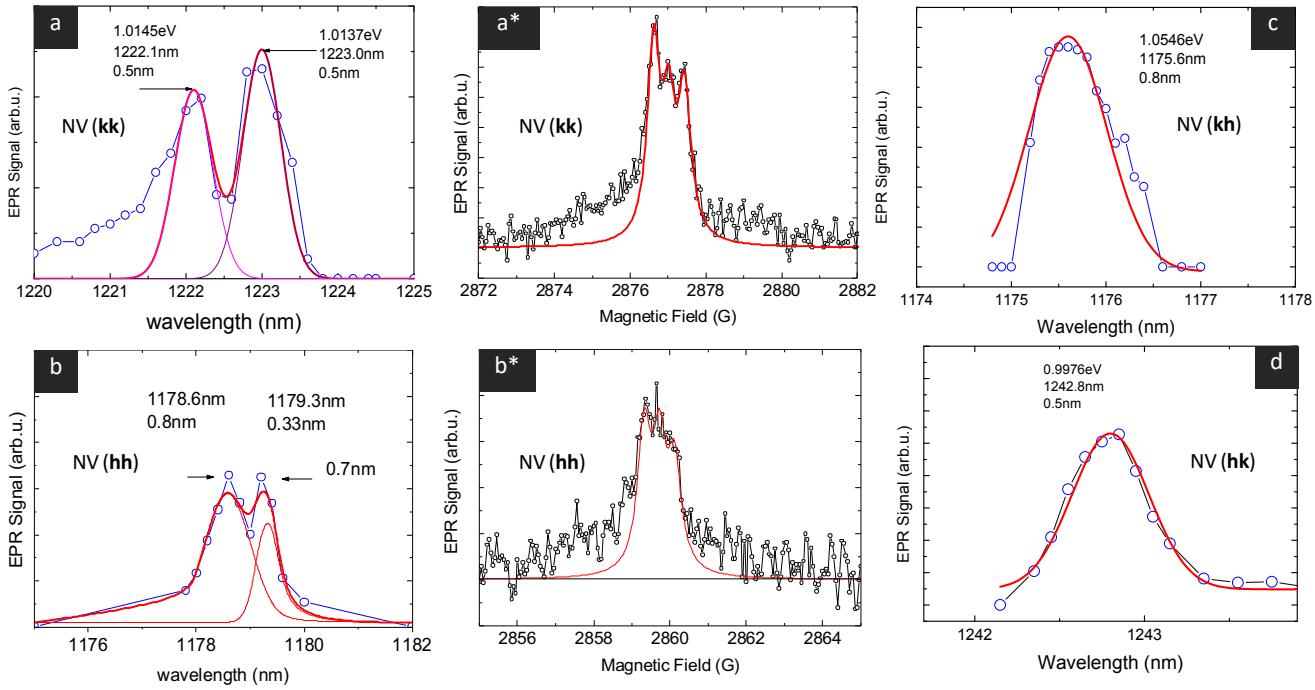

FIG. 6. (a, b) Low temperature (LT), high resolution photoexcitation EPR spectra of the *axial* centers NV(kk), NV(hh) showing both doublet-split ZPL at 1223 nm and 1179 nm, respectively. For comparison (a*, b*), the corresponding LT EPR spectra observed under resonant excitation are given with fitted triplet structures (red) due to the ^{14}N hyperfine interaction (hf) with the associated electron spin of NV^-. Finally in (c, d), the unsplit LT high resolution photoexcitation EPR spectra of the *basal* centers NV(kh), NV(hk) are shown with ZPL at 1175.6 nm and 1242.5 nm, respectively.

However, we do observe a broad excitation spectrum with a threshold at 1223 nm. As the spectral resolution of the laser is below 0.1 nm we then fine scanned the threshold region with a resolution of 0.1 nm. Thereby we observe (Fig. 6a) a sharp ZPL at 1223 nm, which due to the high resolution of the laser excitation shows a resolved doublet fine-structure with two lines of width of 0.5 nm and a splitting of 0.8 nm. The same doublet structure has also been observed in the PL spectrum. The EPR spectrum of the kk center with its characteristic resolved ^{14}N hyperfine interaction observed for the excitation at 1223 nm is shown in Fig. 6a*. The second axial NV center (hh), the resonance field of which is at 2862 G under this condition, is not observed for this excitation. When repeating the high resolution (0.1 nm) photoexcitation for the axial NV(hh) center, we observe again a narrow ZPL, which is situated at 1179 nm and is equally split into a doublet with individual line width of 0.5 nm and a splitting of 0.7 nm (Fig. 6b). The EPR spectrum observed for this resonant excitation is shown in Fig. 6b*; the ^{14}N hyperfine interaction is once again well resolved for the NV(hh) center. We repeated the same procedure for the basal NV centers and we detect for each center a single ZPL line, which are at 1175.6 nm (Fig. 6c) and at 1242.8 nm (Fig. 6d) with linewidth of 0.7 and 0.6 nm, respectively.

In Fig. 7, we compare the ZPL absorption lines with the PL ZPL emission lines measured in the same sample: within experimental resolution, we observe that (*i*) excitation is resonant with basically no shift between the absorption and emission ZPL lines and (*ii*) in the photoexcitation spectrum we observe the same doublet substructure as observed in PL for the ZPL at 1223 nm and 1180 nm.

IV. DISCUSSION

The comparison of the ZPL PL spectra and the EPR photoexcitation spectra show that both agree in wavelength and line-shape (doublet splitting), eventhough the EPR photoexcitation spectra monitor the ZPL absorption spectra.

This feature in combination with the center specific EPR parameters allow us to assign directly the emission ZPL lines to their respective NV centers (Table II). The fact that the excitation is resonant with the emission is a priori surprising as the NV center in diamond provides a Stokes-shift of about 200 meV[28,29]. Also in SiC, previous calculations for the neutral divacancy center, which has a similar electronic structure, predict a Franck-Condon shift of about 50 meV[6,30]; this is not observed here for the NV centers. On the other hand we should keep in mind, however, that resonant absorption with no Franck-

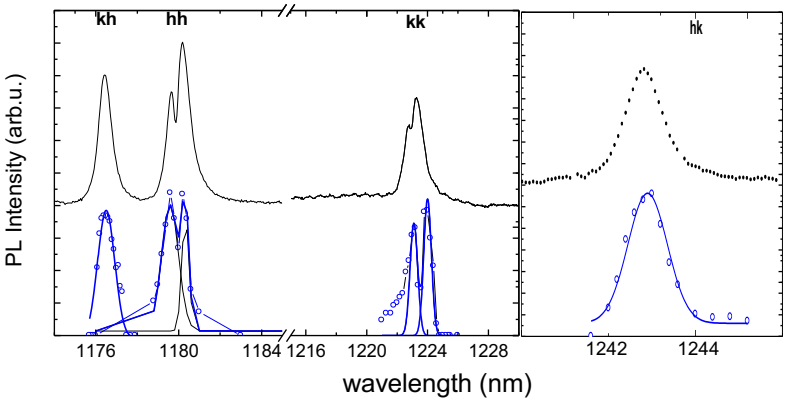

FIG. 7. Comparison of low temperature photoluminescence ZPL lines (top) and EPR tagged photoexcitation spectra (bottom).

Condon shift has also been reported for the negatively charged Si monovacancy[17]. In that work a variant of directly detected time-resolved EPR has been used together with high resolution optical excitation. Most photoexcitation EPR measurements have, however, either been performed non-resonantly or when resonant excitation has been employed the detection has been performed via the broad phonon sidebands. In the present case, with four very similar ZPL energies, the sidebands from all the four centers will be overlapping and wipe out the selectivity obtainable with resonant excitation and non-PL detection. In this sense the EPR tagged photoexcitation spectroscopy is quite unique as the high spectral resolution is conserved and additional defect parameters can be associated with the optical spectra at the same time.

To interpret the doublet structure of the ZPL of the axial centers different hypotheses can be put forward. A splitting of 0.7 nm at 1223 nm corresponds to a frequency splitting of 150 GHz (0.6 meV), which is of course much higher than the zero-field splitting (cf. Table II) and also considerably higher than spin-spin and spin-orbit splitting, which by comparison with the case of the divacancies in 4*H*-SiC are expected clearly in the below 25 GHz range[31]. The doublet structure might thus be an indication of a second excited state which is expected from theory[23], but an exact calculation of its energy appears out of the scope for such calculations and require more elaborate techniques including configuration interaction (CI)[26]. A second scenario would be to imply strain effects which can give rise to splitting of the excited ^{3}E state of tens of GHz[31]. Indeed, as the ^{3}E excited state is an orbital doublet, its degeneracy is lifted by non-axial strain into two orbital branches, E_x and E_y, each orbital branch being formed by three spin states S_x, S_y, and S_z. As our samples have been irradiated at high fluences, we can expect to have high strain effects as has been shown for example for the NV center in diamond. Here, the strain distribution on individual NV centers has been measured as a function of ion implantation conditions[32] and a resulting splitting of the ZPL has equally been observed[33]. At this point we cannot favor or exclude any of the two possibilities. Most probably several effects contribute (even with different sign) to the exact value of the doublet splitting.

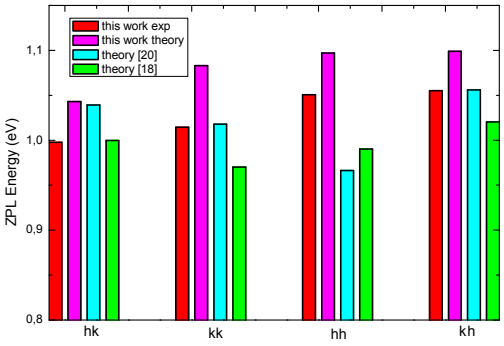

FIG. 8. ZPL energies of the NV centers in 4*H*-SiC as proposed previously by theory for adiabatic emission (Ref. 21 in *green*; Ref. 23 in *light blue*). For comparison vertical excitation energies calculated in this work (*magenta*) are also shown.

We now compare the energies of the emission ZPL of the NV centers in 4*H*-SiC which have been reported in two first principle calculations[21,23] with our experimental results. The energies of the corresponding absorption ZPL lines had not been given in these previous works. In Fig. 8 we superpose the calculated emission ZPL wavelength with the measured absorption/emission ZPL lines now directly assigned. We see that the discrepancy is still rather high both between experiment and theory and even between the two theory works (light blue and green columns). Even though the theoretical values are in the correct range around 1220 nm, it is evident that the results critically depend on technical details used in the calculations, so that the precision of these calculations is still not sufficient to attribute the ZPL emission to specific NV centers without additional information. Very recently Davidsson et al.[25] have analyzed the difficulties to obtain such values with high precision by investigating the influence of the supercell size, the chosen functional and the k-point sampling, using the divacancies (VV) in 4H-SiC as a prototype example. The ZPL emission en-

TABLE II. Spin Hamiltonian parameters of the NV- center in 4*H*-SiC: ZPL, zero field splittings D, ansisotropy parameter E (vanishing for axial centers), ^{14}N hyperfine interactions $A^{\rm exp}$ for B//c. The attribution to *specific* axial (hh or kk) and basal centers (kh or hk) relies on their specific D-value (cf. Ref. 22). Theoretical hyperfine splittings $A^{\rm DFT}$(MHz) are equally given, also for some experimentally unresolved ^{29}Si and ^{13}C hyperfine interactions (all data for B//c).

ZPL(nm)	model	D(MHz)	E(MHz)	$\lvert A^{\rm exp}\rvert$ $1\times^{14}$N (MHz)	$A^{\rm DFT}$ $1\times^{14}$N (MHz)	$A^{\rm DFT}$ $6\times^{29}$Si (MHz)	$A^{\rm DFT}$ $3\times^{29}$Si (MHz)	$A^{\rm DFT}$ $3\times^{13}$C (MHz)	symmetry
1222.1 / 1223.0	NV (kk)	1282	0	1.12	–1.15	9.1	11.1	63.7	C_{3V}
1178.6 / 1179.3	NV (hh)	1331	0	1.23	–1.09	8.1	10.4	69.0	C_{3V}
1242.8	NV (hk)	1193	104	—	–0.56	7.0 (2×)	9.3 (1×)	124 (1×)	C_{1h}
						9.2 (4×)	7.0 (2×)	68 (2×)	
1175.6	NV (kh)	1328	15	—	–0.84	7.9 (2×)	9.1 (1×)	132 (1×)	C_{1h}
						10.1 (4×)	7.8 (2×)	70 (2×)	

ergies of the divacancies change by more than 100 meV when the supercell size is increased from 400 to 1600 atoms. Even more important, the order of axial/basal ZPL lines changes also with the supercell size, with the basal VV centers having the lowest energy for cell sizes of 400 atoms but becoming the higher energy ZPL for the largest supercells. Similar changes of the energetic order are found by varying the k-point sampling and the XC-functional, in particluar if the ZPL lines become energetically close. It was, thus, concluded that in general without additional parameters (HF splitting, zero field splitting) it will not be possible to associate the ZPL lines to a particular axial/basal configuration as their energy difference is only of the order of a few meV.

Motivated by the vanishing Stokes-shift observed experimentally, we calculate the vertical excitation energies for the four NV configurations within constraint DFT using the *Quantum* ESPRESSO package[34]. Thereby, the $^3A_2$ ground state geometries have been used together with an excited occupation of the one-particle levels reflecting the ^3E character of the excited state. Technically, the calculations have been done following the same procedure used in Ref. 20 for the ZPL emission energies. While using supercells of hexagonal shape and shifted k-point samplings convergence of absorption energies seems to be obtained for 768 atoms, at least for the energetic order of the NV configurations (see Table III and magenta columns in Fig. 8). This is particularly remarkable having in mind the more critical convergence behavior of the adiabatic ZPL emission energies and raises the validity of the Franck-Condon concept to be questionable in this case. In any case, our approach, in which we combine high resolution photoexcitation with EPR spectra analysis of centers with distinct Spin Hamiltonian parameters (cf. also Table II) overcomes all these difficulties in the theoretical predictions, while establishing a 1:1 relation of EPR signals to a given ZPL line.

TABLE III. Calculated absorption energies for the vertical ^{3}A$_2$ $\rightarrow^3$E excitation of the NV$^-$ centers in 4*H*-SiC (*768 atom supercell of hexagonal shape*) in comparison with the experimental ZPL energies determined in this work via resonant photoexcitation EPR.

model	exp. (eV)	PBE (eV)	HSE (eV)
kh	1.055	0.974	1.099
hh	1.051	0.975	1.097
kk	1.014	0.959	1.083
hk	0.998	0.919	1.043

V. CONCLUSION

In this work, EPR tagged high resolution photoexcitation spectroscopy has been used to unravel the relation of a series of ZPL lines in the near infrared to specific configurations of the $N_C V_{Si}^-$ pairs. The formation and identification of the NV centers in Silicon Carbide, as well as their attribution to specific EPR signatures had been achieved before[20,22], but the association of the related optical ZPL lines was not yet settled: a conclusive assignment of the ZPL lines to specific NV centers based on theoretical predictions of the transition energies alone is not possible due to their small differences in energy (meV) partially falling into the error bars of their theoretical predictions[25,30]. Based on the simultaneous measurement of the zero phonon absorption line and the related zero-field splitting (ZFS) parameter by EPR tagged photoexcitation spectroscopy we have been able to overcome this difficulty and have refined the assignment of the ZPL photoluminescence lines of the four different NV centers in 4*H*-SiC. Note that this assignment is made without referring to any calculated ZPL energy; their calculation within sufficient accuracy still provides a major challenge for theory.

We have further shown that the ZPL absorption lines have a width of only 0.5 nm and are resonant with the ZPL emission lines. Thus, single defects spectroscopy and selective adressing of individual NV centers should be readily achieved. More generally, our results show that cw-EPR tagged high resolution excitation spectroscopy is a very promising approach for the

association of ZPL spectra with specific defect centers; this approach will certainly find further application in microwave or electrically detected defect spectroscopy and will motivate further investigation in semiconductor materials for emerging quantum technologies.

ACKNOWLEDGMENTS

We thank F. Margaillan (INSP, Sorbonne Université) for his competent contribution to the PL measurements. Visiting scientist S.A.Z wishes to acknowledge the generous support from the international Merlion grant France-Singapour and the Quantum Nanophotonic Laboratories at NTU Division of Physics and Applied Physics, School of Physical and Mathematical Sciences. The authors gratefullky acknowledge financial support from the Merlion program France Singapore n 2.06.16 and from Deutsche Forschungsgemeinschaft (DFG) via Priority Program SPP-1601.

* vonbarde@insp.jussieu.fr
† uwe.gerstmann@uni-paderborn.de
‡ Visiting Scientist at Quantum Nanophotonic Labotaries, Nanyang Technical University (NTU), Sinpapore

[1] M. W. Doherty, N. B. Manson, P. Delaney, F. Jelezko, J. Wrachtrup, and L. C. L. Hollenberg, physics reports **528**, 1 (2013).
[2] J. R. Weber, W. F. Koehl, J. B. Varley, A. Janotti, B. B. Buckley, C. G. Van de Walle, and D. D. Awschalom, Proceedings of the National Academy of Sciences **107**, 8513 (2010).
[3] J. R. Weber, W. F. Koehl, J. B. Varley, A. Janotti, B. B. Buckley, C. G. Van de Walle, and D. D. Awschalom, Journal of Applied Physics **109**, 102417 (2011).
[4] A. Dzurak, Nature **479**, 47 (2011).
[5] A. Boretti, Nature Photonics **8**, 88 (2014).
[6] L. Gordon, A. Janotti, and C. G. Van de Walle, Physical Review B **92**, 045208 (2015).
[7] O. V. Zwier, D. O'Shea, A. R. Onur, and C. H. van der Wal, Scientific Reports **5**, 10931 (2015).
[8] D. Riedel, F. Fuchs, H. Kraus, S. Väth, A. Sperlich, V. Dyakonov, A. A. Soltamova, P. G. Baranov, V. A. Ilyin, and G. V. Astakhov, Physical Review Letters **109**, 226402 (2012).
[9] V. A. Soltamov, A. A. Soltamova, P. G. Baranov, and I. I. Proskuryakov, Physical Review Letters **108**, 226402 (2012).
[10] M. Widmann, S.-Y. Lee, T. Rendler, N. T. Son, H. Fedder, S. Paik, L.-P. Yang, N. Zhao, S. Yang, I. Booker, A. Denisenko, M. Jamali, S. A. Momenzadeh, I. Gerhardt, T. Ohshima, A. Gali, E. Janzén, and J. Wrachtrup, Nature Materials (2014), 10.1038/nmat4145.
[11] S. G. Carter, Ö. O. Soykal, P. Dev, S. E. Economou, and E. R. Glaser, Physical Review B **92**, 161202 (2015).
[12] D. J. Christle, A. L. Falk, P. Andrich, P. V. Klimov, J. U. Hassan, N. T. Son, E. Janzén, T. Ohshima, and D. D. Awschalom, Nature Materials **14**, 160 (2015).
[13] P. V. Klimov, A. L. Falk, D. J. Christle, V. V. Dobrovitski, and D. D. Awschalom, Science Advances **1**, e1501015 (2015).
[14] D. Simin, H. Kraus, A. Sperlich, T. Ohshima, G. V. Astakhov, and V. Dyakonov, Physical Review B **95**, 161201 (2017).
[15] Y. Zhou, J. Wang, X. Zhang, K. Li, J. Cai, and W. Gao, Physical Review Applied **8**, 044015 (2017).
[16] E. Sörman, N. Son, W. Chen, O. Kordina, C. Hallin, and E. Janzén, Physical Review B **61**, 2613 (2000).
[17] P. G. Baranov, A. P. Bundakova, A. A. Soltamova, S. B. Orlinskii, I. V. Borovykh, R. Zondervan, R. Verberk, and J. Schmidt, Phys. Rev. B **83**, 125203 (2011).
[18] V. A. Soltamov, B. V. Yavkin, D. O. Tolmachev, R. A. Babunts, A. G. Badalyan, V. Y. Davydov, E. N. Mokhov, I. I. Proskuryakov, S. B. Orlinskii, and P. G. Baranov, Phys. Rev. Lett. **115**, 247602 (2015).
[19] U. Gerstmann, E. Rauls, T. Frauenheim, and H. Overhof, Phys. Rev. B **67**, 205202 (2003).
[20] H. J. Von Bardeleben, J. L. Cantin, E. Rauls, and U. Gerstmann, Physical Review B **92**, 064104 (2015).
[21] S. A. Zargaleh, B. Eble, S. Hameau, J. L. Cantin, L. Legrand, M. Bernard, F. Margaillan, J. S. Lauret, J. F. Roch, H. J. Von Bardeleben, E. Rauls, U. Gerstmann, and F. Treussart, Physical Review B **94**, 060102 (2016).
[22] H. J. Von Bardeleben, J. L. Cantin, A. Csóré, A. Gali, E. Rauls, and U. Gerstmann, Physical Review B **94**, 121202 (2016).
[23] A. Csóré, H. J. Von Bardeleben, J. L. Cantin, and A. Gali, Physical Review B **96**, 085204 (2017).
[24] H. J. Von Bardeleben and J. L. Cantin, MRS Communications **7**, 591 (2017).
[25] J. Davidsson, V. Ivády, R. Armiento, N. T. Son, A. Gali, and I. A. Abrikosov, New Journal of Physics **20**, 023035 (2018).
[26] M. Bockstedte, F. Schütz, T. Garrat, V. Ivády, and A. Gali, npj Quantum Materials **3**, 1 (2018).
[27] A. L. Falk, B. B. Buckley, G. Calusine, W. F. Koehl, V. V. Dobrovitski, A. Politi, C. A. Zorman, P. X. L. Feng, and D. D. Awschalom, Nature Communications **4**, 1819 (2013).
[28] A. Batalov, V. Jacques, F. Kaiser, P. Siyushev, P. Neumann, L. J. Rogers, R. L. McMurtrie, N. B. Manson, F. Jelezko, and J. Wrachtrup, Phys. Rev. Lett. **102**, 195506 (2009).
[29] G. Thiering and A. Gali, Phys. Rev. B **96**, 081115 (2017).
[30] A. Beste and D. E Taylor, *Convergence of Ground and Excited State Properties of Divacancy Defects in 4H-SiC with Computational Cell Size*, Tech. Rep. ARL-TR-8313 (2018).
[31] D. J. Christle, P. V. Klimov, C. F. d. l. Casas, K. Szász, V. Ivády, V. Jokubavicius, J. U. Hassan, M. Syväjärvi, W. F. Koehl, T. Ohshima, N. T. Son, E. Janzén, A. Gali, and D. D. Awschalom, Phys. Rev. X **7**, 021046 (2017).

[32] Y. Chu, N. P. de Leon, B. J. Shields, B. Hausmann, R. Evans, E. Togan, M. J. Burek, M. Markham, A. Stacey, A. S. Zibrov, A. Yacoby, D. J. Twitchen, M. Loncar, H. Park, P. Maletinsky, and M. D. Lukin, Nano Lett **14**, 1982 (2014).

[33] P. Olivero, F. Bosia, B. A. Fairchild, B. C. Gibson, A. D. Greentree, P. Spizzirri, and S. Prawer, New Journal of Physics **15**, 043027 (2013).

[34] P. Giannozzi, S. Baroni, N. Bonini, M. Calandra, R. Car, C. Cavazzoni, D. Ceresoli, G. L. Chiarotti, M. Cococcioni, I. Dabo, A. Dal Corso, S. de Gironcoli, S. Fabris, G. Fratesi, R. Gebauer, U. Gerstmann, C. Gougoussis, A. Kokalj, M. Lazzeri, L. Martin-Samos, N. Marzari, F. Mauri, R. Mazzarello, S. Paolini, A. Pasquarello, L. Paulatto, C. Sbraccia, S. Scandolo, G. Sclauzero, A. P. Seitsonen, A. Smogunov, P. Umari, and R. M. Wentzcovitch, Journal of Physics, Condensed Matter **21**, 395502 (2009).